Automated whole-cell patch clamp electrophysiology of neurons *in vivo*

Suhasa B. Kodandaramaiah[1,2], **Giovanni Talei Franzesi**[1], **Brian Y. Chow**[1], **Edward S. Boyden**[1,*], and **Craig R. Forest**[2,*]

[1]MIT Media Lab, McGovern Institute, Dept. of Biological Engineering, and Dept. of Brain and Cognitive Sciences, MIT, Cambridge, MA

[2]George W. Woodruff School of Mechanical Engineering, Georgia Institute Of Technology, Atlanta, GA

Abstract

Whole-cell patch clamp electrophysiology of neurons is a gold standard technique for high-fidelity analysis of the biophysical mechanisms of neural computation and pathology but it requires great skill to perform. We have developed a robot that automatically performs patch clamping *in vivo*, algorithmically detecting cells by analyzing the temporal sequence of electrode impedance changes. We demonstrate good yield, throughput, and quality of automated intracellular recording in mouse cortex and hippocampus.

Whole-cell patch clamp recordings[1, 2] of the electrical activity of neurons *in vivo* utilizes glass micropipettes to establish electrical and molecular access to the insides of neurons in intact tissue. This methodology exhibits signal quality and temporal fidelity sufficient to report the synaptic and ion-channel mediated subthreshold membrane potential changes that enable neurons to compute information, and that are affected in brain disorders or by drug treatment. In addition, molecular access to the cell enables infusion of dyes for morphological visualization, as well as extraction of cell contents for transcriptomic single-cell analysis[3], which together enable the integrative analysis of molecular, anatomical, and electrophysiological properties of single cells in the intact brain. However, *in vivo* patching requires skill, being something of an art to perform, and is laborious. This has posed a challenge for its broad adoption in neuroscience and biology, and precluded systematic or scalable *in vivo* experiments.

We have discovered that unbiased, non-image-guided, *in vivo* whole-cell patching ('blind' patch clamping) of neurons (Fig. 1a), in which micropipettes are lowered until a cell is detected and then an opening in the cell membrane created for intracellular recording, can be reduced to a reliable algorithm. The patch algorithm takes place in four stages (Fig. 1a): "regional pipette localization," in which the pipette is rapidly lowered to a desired depth under positive pressure; "neuron hunting," in which the pipette is advanced more slowly at lower pressure until a neuron is detected, as reflected by a specific temporal sequence of

Correspondence to: Craig R. Forest, Georgia Institute of Technology, 813 Ferst Dr, Room 411, Atlanta, GA 30332, cforest@gatech.edu, Office phone: (404) 385-7645 and Edward S. Boyden, Massachusetts Institute of Technology, E15-421, 20 Ames St., Cambridge, MA 02139, esb@media.mit.edu, Office phone: (650) 468-5625.

Authors' Contributions
S.B.K., B.Y.C, E.S.B. and C.R.F. designed devices and experiments and wrote the paper. S.B.K. conducted experiments. G.T.F. assisted with experiments and autopatcher pilot testing.

Competing financial interests
The authors declare no competing financial interests.

electrode impedance changes; "gigaseal formation," in which the pipette is hyperpolarized and suction applied to create the gigaseal; and "break-in," in which a brief voltage pulse ("zap") is applied to the cell to establish the whole cell state. We constructed a simple automated robot to perform this algorithm (Fig. 1b), which actuates a set of motors and valves rapidly upon recognition of specific temporal sequences of microelectrode impedance changes, achieving in vivo patch clamp recordings in a total period of 3–7 minutes of robot operation. The robot is relatively inexpensive, and can easily be appended to an existing patch rig. We demonstrate the utility of this autopatching robot in obtaining high-quality recordings, which could be held for an hour or longer, in the cortex and hippocampus of anesthetized mouse brain.

The robot (Fig. 1b) monitors pipette resistance as the pipette is lowered into the brain, and automatically moves the pipette in incremental steps via a linear actuator. In principle, the pipette resistance monitoring can be performed by a traditional patch amplifier and digitizer, and the 3 axis linear actuator typically used for in vivo patching can be used as the robotic actuator; we here for flexibility added an additional computer interface board to support pipette resistance monitoring, and an additional linear actuator for pipette movement. The robot also contains a set of valves connected to pressure reservoirs to provide positive pressure during pipette insertion into the brain, as well as negative pressure as necessary to result in gigaseal formation and attainment of the whole cell state (see Supplementary Fig. 1 for details).

The algorithm derivation took place in the cortex, and the validation of the algorithm then took place in both cortex and hippocampus, to confirm generality. After the "regional pipette localization" stage, pipettes that undergo increases of resistance of greater than 300 kΩ after this descent to depth are rejected, which greatly increases the yield of later steps (Supplementary Note 1). During "neuron hunting," the key indicator of neuron presence is that as the pipette is lowered into the brain in a stepwise fashion, there is a monotonic increase in pipette resistance across several consecutive steps (e.g., a 200–250 kΩ increase in pipette resistance across three 2 μm steps). Successfully detected neurons also exhibited an increase in heartbeat modulation of the pipette current (Supplementary Fig. 2, as has been noted before[2], although we did not utilize this in our current version of the algorithm due to the variability in the shape and frequency of the heartbeat from cell to cell (Supplementary Note 1). "Gigaseal formation" was implemented as a simple feedback loop, introducing negative pressure and hyperpolarization of the pipette as needed to form the seal. Finally, "break-in" was implemented through the application of suction and the application of a "zap" voltage pulse to enable the whole-cell state. Information about the algorithm are indicated in **Online Methods**, Supplementary Fig. 3 and Supplementary Note 1. Detailed instructions for robot construction are described in **Supplementary Software (Autopatcher User Manual)**.

We validated the algorithm and robot on targets within the cortex and hippocampus of anesthetized mice,. The robot running the algorithm (Fig. 1a, b, Supplementary Fig. 3), obtained successful whole-cell patch recordings 32.9% of the time (Supplementary Table 1; defined as < 500 pA of current when held at −65 mV, for at least 5 minutes; $n = 24$ out of 73 attempts), and successful gigaseal cell-attached patch clamp recording 36% of the time (defined as a stable seal of >1 GΩ resistance; $n = 27$ out of 75 attempts), success rates that are similar to, or exceed, those of a trained investigator manually performing blind whole-cell patch clamping *in vivo* (for us, 28.8% success at whole-cell patching; $n = 17$ out of 59 fully manual attempts; see also refs.[2, 4, 5]). Example traces from neurons autopatched in cortex and hippocampus are shown in Fig. 1c,d. When biocytin was included in the pipette solution, morphologies of cells could be visualized (Fig. 1e and Supplementary Fig. 4) histologically. Focusing on the robot's performance after the "regional pipette localization"

stage (i.e., leaving out losses due to pipette blockage during the descent to depth), the autopatcher was successful at whole-cell patch clamping 43.6% of the time (Supplementary Table 1; $n = 24$ out of 55 attempts starting with the "neuron hunting" stage), and at gigaseal cell-attached patch clamping 45.8% of the time ($n = 27$ out of 59 attempts). Of the successful recordings described in the previous paragraph, approximately 10% were putative glia, as reflected by their capacitance and lack of spiking[6] (4 out of 51 successful autopatched recordings; 2 out of 17 successful fully manual recordings). For simplicity, we analyzed just the neurons, in the rest of the paper; their various firing patterns are described in the Supplementary Note 2. From the beginning of the neuron-hunting stage, to acquisition of successful whole-cell or gigaseal cell-attached recordings, took 5 ± 2 minutes for the robot to perform (Supplementary Table 1), not significantly different from the duration of fully manual patching (5 ± 3 minutes; p = 0.7539; $n = 47$ autopatched neurons, 15 fully manually patched neurons).

A representative autopatcher run, plotting the pipette resistance versus time, is shown in Fig. 2a, with key events indicated by Roman numerals; raw current traces resulting from the continuously applied voltage pulses, from which the pipette resistances were derived, are shown in Fig. 2b. Note the small visual appearance of the change in pipette currents observed when a neuron is detected (Fig. 2b, event **ii**). See **Online methods** for details of the autopatcher timecourse and execution. The quality of cells recorded by the autopatcher was comparable to those in published studies conducted by skilled human investigators[2, 4, 7–9], and to our own fully manually patched cells (Fig. 2c–f, Supplementary Fig. 5). These comparisons showed no statistically significant difference between n = 23 auto-whole-cell patched and n = 15 fully manually patched neurons for access resistance, holding current, resting membrane potential, holding time, gigaseal resistance, cell membrane capacitance, or cell membrane resistance (detailed statistics in Supplementary Notes 3 and 4).

Once the robot has been assembled, it is easy to use it to derive alternative or specialized algorithms (e.g., if a specialized cell type is the target, or if image-guided or other styles of patching is desired, or if the technology is desired to be combined with other technologies such as optogenetics for cell-type identification[10]). As an example, we derived a variant of the algorithm that uses pulses of suction to break in to cells, rather than "zap" (Supplementary Fig. 6); the yields, cell qualities, and cell properties obtained by the suction-pulse variation of the autopatch algorithm were comparable to those obtained by the original algorithm (Supplementary Fig. 7). The inherent data logging of the robot allows fine-scale analyses of the patch process, for example revealing that the probability of success of autopatching starts at 50–70% in the first hour, and then drops to 20–50% over the next few hours, presumably due to cellular displacement intrinsic to the *in vivo* patching process (Supplementary Fig. 7d).

We have developed a robot that automatically performs patch clamping *in vivo*, algorithmically detecting cells by analyzing the temporal sequence of electrode impedance changes, and demonstrated it in the cortex and hippocampus of live mice. We anticipate that other applications of robotics to the automation of *in vivo* neuroscience experiments, and to other *in vivo* assays in bioengineering and medicine, will be possible. The ability to automatically make micropipettes in a high-throughput fashion[11], and to install them automatically, might eliminate some of the few remaining steps requiring human intervention. The use of automated respiratory and temperature monitoring could enable a single human operator to control many rigs at once, increasing throughput further (see Supplementary Note 5 for discussion of throughput). As a final example, the ability to control many pipettes within a single brain, and to perform parallel recordings of neurons

within a single brain region, may open up new strategies for understanding how different cell types function in the living milieu.

Online Methods

Surgical procedures

All animal procedures were approved by the Massachusetts Institute of Technology (MIT) Committee on Animal Care. Adult male C57BL/6 mice, 8–12 weeks old, were purchased from Taconic.Upon arrival, the mice were housed in standard cages in the MIT animal facility with ad libitum food and water in a controlled light-dark cycle environment, with standard monitoring by veterinary staff, for the period before the experiment. On the day of the experiment, they were anesthetized using ketamine/xylazine (initially at 100 mg/kg and 10 mg/kg, and redosed at 30–45 minute intervals with 10–15% of the initial ketamine dose as needed, using toe pinch reflex as a standard metric of anesthesia depth). The scalp was shaved, and the mouse placed in a custom stereotax, with ophthalmic ointment applied to the eyes, and with Betadine and 70% ethanol used to sterilize the surgical area. Three self-tapping screws (F000CE094, Morris Precision Screws and Parts) were attached to the skull and a plastic headplate affixed using dental acrylic, as previously described[12]. Once set (~20 minutes), the mice were removed from the stereotactic aparatus and placed in a custom-built low profile holder. A dental drill was used to open up one or more craniotomies (1–2 mm diameter) by thinning the skull until ~100 μm thick, and then a small aperture was opened up with a 30 gauge needle tip. Cortical craniotomies occurred at stereotaxic coordinates: anteroposterior, 0 mm relative to bregma; mediolateral, 0–1 mm left or right of the midline; neuron hunting began at 400 μm depth. Hippocampal craniotomies occurred at stereotaxic coordinates: anteroposterior, –2 mm relative to bregma; mediolateral, 0.75–1.25 mm left or right of the midline; neuron hunting began at 1100 μm depth. It is critical to ensure that bleeding is minimal and the craniotomy is clean, as this allows good visualization of the pipette, and minimizes the number of pipettes blocked after insertion into the brain. The dura was removed using a pair of fine forceps. The craniotomy was superfused with artificial cerebrospinal fluid (ACSF, consisting of 126 mM NaCl, 3 mM KCl, 1.25 mM NaH_2PO_4, 2 mM $CaCl_2$, 2 mM $MgSO_4$, 24 mM $NaHCO_3$, and 10 mM glucose), to keep the brain moist until the moment of pipette insertion.

17 mice were used to derive the autopatching algorithm (Supplementary Fig. 2). 16 mice were used to validate the robot for the primary test-set (Fig. 2, Supplementary Fig. 3a and Supplementary Fig. 3b). For the manual experiments (Fig. 2c–f and Supplementary Fig. 3c), we used 4 mice. For the development of the suction-based autopatching variant (Supplementary Fig. 5, 6), we used 5 mice. Out of the 5 mice used for suction-based autopatching, 3 mice were used for the throughput estimations (Supplementary Note 6). For biocytin filling experiments (Fig. 1f and Supplementary Fig. 4) and validation of heartbeat modulation as a method for confirming neuronal detection (Supplementary Note 1), we used 6 additional mice.

At the end of the patch clamp recording, mice were euthanized, while still fully anesthetized, via cervical dislocation, unless biocytin filling was attempted. In the case of biocytin filling, the mice were isoflurane anesthetized, then transcardially perfused in 4% ice-cold through the left cardiac ventricle with ~40 mL of ice-cold 4% paraformaldehyde in phosphate buffered saline (PBS) (see **Histology and Imaging** section for more details).

Electrophysiology

Borosilicate glass pipettes (Warner) were pulled using a filament micropipette puller (Flaming-Brown P97 model, Sutter Instruments), within a few hours before beginning the

experiment, and stored in a closed petri dish to reduce dust contamination. We pulled glass pipettes with resistances between 3–9 MΩ. The intracellular pipette solution consisted of (in mM): 125 potassium gluconate (with more added empirically at the end, to bring osmolarity up to ~290 mOsm), 0.1 $CaCl_2$, 0.6 $MgCl_2$, 1 EGTA, 10 HEPES, 4 Mg ATP, 0.4 Na GTP, 8 NaCl (pH 7.23, osmolarity 289 mOsm), similar as to what has been used in the past[13]. For experiments with biocytin, 0.5% biocytin (weight/volume) was added to the solution before the final gluconate-based osmolarity adjustment, and osmolarity then adjusted (to 292 mOsm) with potassium gluconate. We performed manual patch clamping using previously described protocols[2, 9], with some modifications and iterations as explained in the text, in order to prototype algorithm steps and to test them.

Robot construction

We assembled the autopatcher (Fig. 1b,c) through modification of a standard *in vivo* patch clamping system. The standard system comprised a 3-axis linear actuator (MC1000e, Siskiyou Inc) for holding the patch headstage, and a patch amplifier (Multiclamp 700B, Molecular Devices) that connects its patch headstage to a computer through a analog/digital interface board (Digidata 1440A, Molecular Devices). For programmable actuation of the pipette in the vertical direction, we mounted a programmable linear motor (PZC12, Newport) onto the 3-axis linear actuator. For experiments where we attempted biocytin filling, we mounted the programmable linear motor at a 45° angle to the vertical axis, to reduce the amount of background staining in the coronal plane that we did histological sectioning along. The headstage was in turn mounted on the programmable linear motor through a custom mounting plate. The programmable linear motor was controlled using a motor controller (PZC200, Newport Inc) that was connected to the computer through a serial COM port. An additional data acquisition (DAQ) board (USB 6259 BNC, National Instruments Inc) was connected to the computer via a USB port, and to the patch amplifier through BNC cables, for control of patch pipette voltage commands, and acquisition of pipette current data, during the execution of the autopatcher algorithm. During autopatcher operation, the USB 6259 board sent commands to the patch amplifier; after acquisition of cell-attached or whole-cell-patched neurons, the patch amplifier would instead receive commands from the Digidata; we used a software-controlled TTL co-axial BNC relay (CX230, Tohtsu) for driving signal switching between the USB 6259 BNC and the Digidata, so that only one would be empowered to command the patch amplifier at any time. The patch amplifier streamed its data to the analog input ports of both the USB DAQ and the Digidata throughout and after autopatching. For pneumatic control of pipette pressure, we used a set of three solenoid valves (2-input, 1-output, LHDA0533215H-A, Lee Company). They were arranged, and operated, in the configuration shown in Supplementary Fig. 1. The autopatcher program was coded in, and run by, Labview 8.6 (National Instruments). Detailed instructions for robot construction are described in the **Supplementary Software (Autopatcher User Manual)**.

The USB6259 DAQ sampled the patch amplifier at 30 KHz and with unity gain applied, and then filtered the signal using a moving average smoothening filter (half width, 6 samples, with triangular envelope), and the amplitude of the current pulses was measured using the peak-to-peak measurement function of Labview. During the entire procedure, a square wave of voltage was applied, 10 mV in amplitude, at 10 Hz, to the pipette via the USB6259 DAQ analog output. Resistance values were then computed, by dividing applied voltage by the peak-to-peak current observed, for 5 consecutive voltage pulses, and then these 5 values were averaged. Once the autopatch process was complete, neurons were recorded using Clampex software (Molecular Devices). Signals were acquired at standard rates (e.g., 30–50 KHz), and low-pass filtered (Bessel filter, 10 KHz cutoff). All data was analyzed using Clampfit software (Molecular Devices) and MATLAB (Mathworks).

Robot Operation

At the beginning of the experiment, we installed a pipette and filled it with pipette solution using a thin polyimide/fused silica needle (Microfil) attached to a syringe filter (0.2 μm) attached to a syringe (1 mL). We removed excess ACSF to improve visualization of the brain surface in the pipette lowering stage, and then applied positive pressure (800–1000 mBar), low positive pressure (25–30 mBar), and suction pressure (−15 to −20 mBar) at the designated ports (Fig. 1, Supplementary Fig. 1) and clamped the tubing to the input ports with butterfly clips; the initial state of high positive pressure was present at this time (with all valves electrically off). We used the 3-axis linear actuator (Siskiyou) to manually position the pipette tip over the craniotomy using a control joystick with the aid of a stereomicroscope (Nikon). The pipette was lowered until it just touched the brain surface (indicated by dimpling of surface) and retracted back by 20–30 micrometers. The autopatcher software then denotes this position, just above the brain surface, as z = 0 for the purposes of executing the algorithm (Supplementary Fig. 2), acquiring the baseline value R(0) of the pipette resistance at this time (the z-axis is the vertical axis perpendicular to the earth's surface, with greater values going downwards). The pipette voltage offset was automatically nullified by the "pipette offset" function in the Multiclamp Commander (Molecular Devices). We ensured that electrode wire in the pipette was chlorided enough so as to minimize pipette current drift which can affect the detection of the small resistance measurements that occur during autopatcher operation. The brain surface was then superfused with ACSF and the autopatcher program was started. See included **Supplementary Software (Autopatcher User Manual)** for detailed description of running the Labview program for autopatching. Updated versions of the software and user manual will be made available online at http://autopatcher.org.

Details of Autopatcher Program Execution

The autopatcher evaluates the pipette electrical resistance is evaluated outside the brain (e.g., between 3–9 MΩ is typical) for 30–60 seconds to see if AgCl pellets or other particulates internally clog the pipette (indicated by increases in resistance). If the pipette resistance remains constant and is of acceptable resistance, the Autopatcher program is started. The program records the resistance of the pipette outside the brain and automatically lowers the pipette to a pre-specified target region within the brain (the stage labeled "regional pipette localization" in Fig. 1a), followed by a second critical examination of the pipette resistance for quality control. This check is followed by an iterative process of lowering the pipette by small increments, while looking for a pipette resistance change indicative of proximity to a neuron suitable for recording (the "neuron hunting" stage). During this stage, the robot looks for a specific sequence of resistance changes that indicates that a neuron is proximal, attempting to avoid false positives that would waste time and decrease cell yield. After detecting this signature, the robot halts movement, and begins to actuate suction and pipette voltage changes so as to form a high-quality seal connecting the pipette electrically to the outside of the cell membrane (the "gigaseal formation" stage), thus resulting in a gigaseal cell-attached recording. If whole-cell access is desired, the robot can then be used to perform controlled application of suction in combination with brief electrical pulses to break into the cell (the "break-in" stage, Supplementary Fig. 3). Alternately, break-in can also be achieved using pulses of suction (Supplementary Fig. 6).

Throughout the process, the robot applies a voltage square wave to the pipette (10 Hz, 10 mV alternating with 0 mV relative to pipette holding voltage), and the current is measured, in order to calculate the resistance of the pipette at a given depth or stage of the process. Throughout the entire process of robot operation, this pipette resistance is the chief indicator of pipette quality, cell presence, seal quality, and recording quality, and the algorithm attempts to make decisions – such as whether to advance to the next stage, or to restart a

stage, or to halt the process – entirely on the temporal trajectory taken by the pipette resistance during the experiment. The performance of the robot is enabled by two critical abilities of the robot: its ability to monitor the pipette resistance quantitatively over time, and its ability to execute actions in a temporally precise fashion upon the measured pipette resistance reaching quantitative milestones.

Focusing on the data for the $n = 47$ neurons in the main validation test set: the neuron-hunting stage took on average 2.5 ± 1.7 minutes ($n = 47$), with the time to find a target that later led to successful gigaseal not differing significantly from the time to find a target that does not lead to a gigaseal ($P = 0.8114$; t-test; $n = 58$ unsuccessful gigaseal formation trials), that is, failed trials did not take longer than successful ones. The gigaseal formation took 2.6 ± 1.0 minutes, including for the whole cell autopatched case the few seconds required for break-in; failed attempts to form gigaseals were truncated at the end of the ramp down procedure and thus took ~85 seconds. These durations are similar to those obtained by trained human investigators practicing published protocols[4].

Histology and Imaging—For experiments with biocytin filling of cells, mice were perfused through the left cardiac ventricle with ~40 mL of ice-cold 4% paraformaldehyde in phosphate buffered saline (PBS) while anesthetized with isoflurane. Perfused brains were then removed from the skull then postfixed overnight in the same solution at 4 °C. The fixed brains were incubated in 30% sucrose solution for 2 days until cryoprotected (i.e., the brains sank). The brains were flash frozen in isopentane cooled using dry ice at temperatures between –30 °C to –40 °C. The flash frozen brains were mounted on mounting plates using OCT as base, and covered with tissue embedding matrix to preserve tissue integrity, and 40 μm thick slices were cut at –20 °C using a cryostat (Leica). The brain slices were mounted on charged glass slides (e.g., SuperFrost) and incubated at room temperature for 4 hours in PBS containing 0.5% Triton-X (vol/vol) and 2% goat serum (vol/vol). This was followed by 12–14 hours of incubation at 4 °C in PBS containing 0.5% Triton-X (vol/vol), 2% goat serum (vol/vol) and Alexa 594 conjugated with streptavidin (Life Technologies, diluted 1:200). After incubation, the slices were thoroughly washed in PBS containing 100 mM glycine and 0.5% Triton-X (vol/vol) followed by washing in PBS with 100 mM glycine. Slices were then mounted in Vectashield with DAPI (Vector Labs), covered using a coverslip, and sealed using nail polish. Image stacks were obtained using a confocal microscope (Zeiss) with 20× objective lens. Maximum intensity projections of the image stacks were taken using ImageJ software. If needed to reconstruct full neuron morphology, multiple such maximum intensity projection images were auto-leveled, then montaged, using Photoshop CS5 software.

Supplementary Material

Refer to Web version on PubMed Central for supplementary material.

Acknowledgments

REFERENCES FOR THE ONLINE METHODS SECTION

1. Hamill OP, Marty A, Neher E, Sakmann B, Sigworth FJ. Improved patch-clamp techniques for high-resolution current recording from cells and cell-free membrane patches. Pflugers Arch. 1981; 391:85–100. [PubMed: 6270629]

2. Margrie TW, Brecht M, Sakmann B. In vivo, low-resistance, whole-cell recordings from neurons in the anaesthetized and awake mammalian brain. Pflugers Arch. 2002; 444:491–498. [PubMed: 12136268]

3. Eberwine J, et al. Analysis of gene expression in single live neurons. Proc Natl Acad Sci U S A. 1992; 89:3010–3014. [PubMed: 1557406]

4. Lee AK, Epsztein J, Brecht M. Head-anchored whole-cell recordings in freely moving rats. Nat. Protocols. 2009; 4:385–392.

5. Kitamura K, Judkewitz B, Kano M, Denk W, Hausser M. Targeted patch-clamp recordings and single-cell electroporation of unlabeled neurons in vivo. Nat Meth. 2008; 5:61–67.

6. Trachtenberg MC, Pollen DA. Neuroglia: Biophysical Properties and Physiologic Function. Science. 1970; 167:1248–1252. [PubMed: 5411911]

7. Harvey CD, Collman F, Dombeck DA, Tank DW. Intracellular dynamics of hippocampal place cells during virtual navigation. Nature. 2009; 461:941–946. [PubMed: 19829374]

8. DeWeese MR, Zador AM. Non-Gaussian membrane potential dynamics imply sparse, synchronous activity in auditory cortex. J Neurosci. 2006; 26:12206–12218. [PubMed: 17122045]

9. DeWeese MR. Whole-cell recording in vivo. Curr Protoc Neurosci. 2007; Chapter 6(Unit 6):22. [PubMed: 18428661]

10. Boyden ES. A history of optogenetics: the development of tools for controlling brain circuits with light. F1000 Biology Reports. 2011; 3

11. Pak N, Dergance MJ, Emerick MT, Gagnon EB, Forest CR. An Instrument for Controlled, Automated Production of Micrometer Scale Fused Silica Pipettes. Journal of Mechanical Design. 2011; 133 061006.

12. Boyden ES, Raymond JL. Active reversal of motor memories reveals rules governing memory encoding. Neuron. 2003; 39:1031–1042. [PubMed: 12971901]

13. Chow BY, et al. High-performance genetically targetable optical neural silencing by light-driven proton pumps. Nature. 2010; 463:98–102. [PubMed: 20054397]
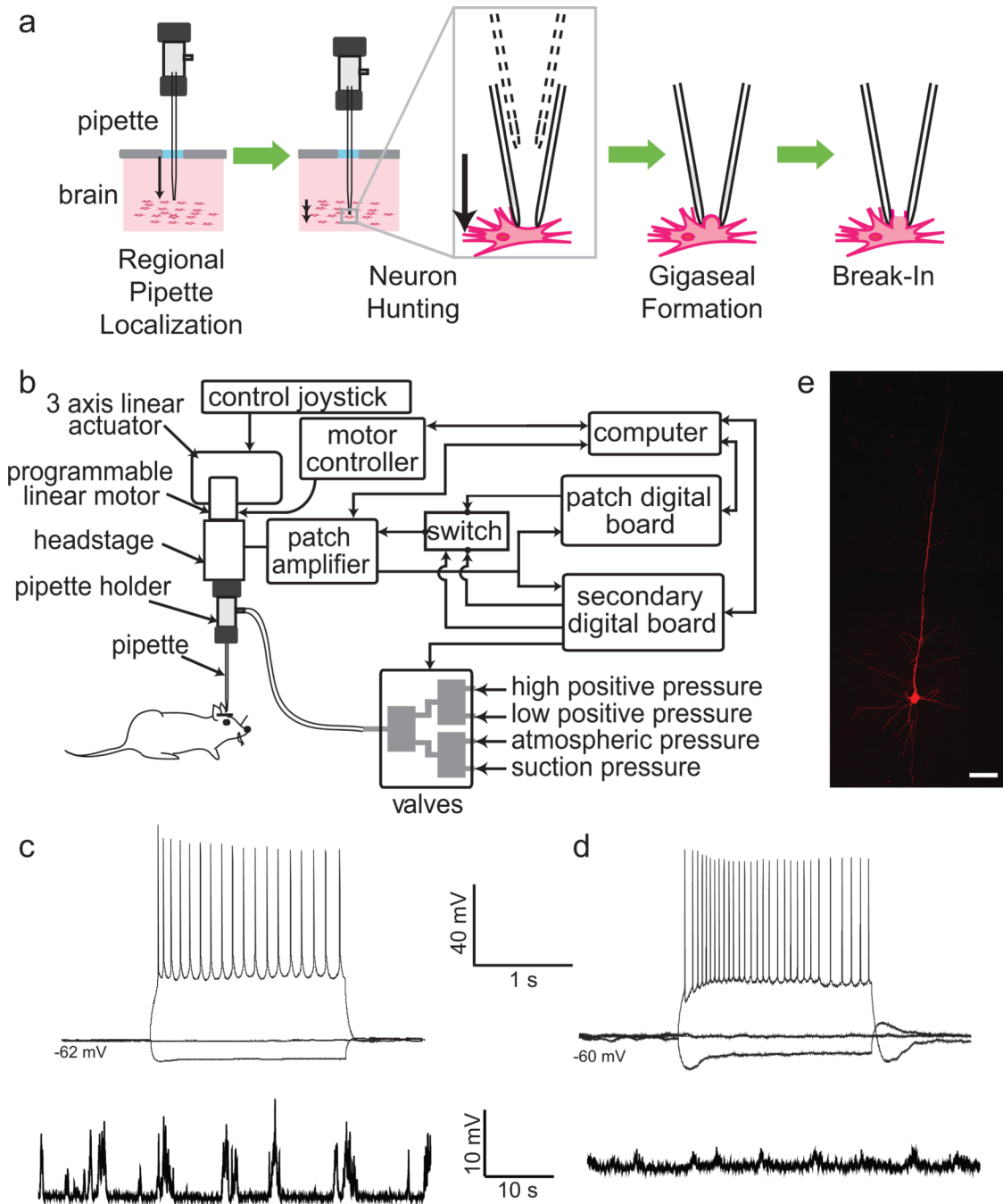
Figure 1. The autopatcher: a robot for *in vivo* patch clamping
(**a**) The four stages of the automated *in vivo* patch algorithm (detailed in Supplementary Fig. 3).(**b**) Schematic of a simple robotic system capable of performing the autopatching algorithm, consisting of a conventional *in vivo* patch setup, equipped with a programmable linear motor (note that if the vertical axis of the 3 axis linear actuator is computer-controlled, this can be omitted), a controllable bank of pneumatic valves for pressure control, and a secondary computer interface board (if the patch amplifier provides direct access to these measurements, this can be omitted). (**c**) Current clamp traces during current injection (*top*; 2 s-long pulses of −60, 0, and +80 pA current injection), and at rest (*bottom*; note compressed

timescale relative to the top trace), for an autopatched cortical neuron. Access resistance, 44 MΩ; input resistance, 41 MΩ; depth of cell 832 μm below brain surface. (**d**) Current clamp traces during current injection (*top*; 2 s-long pulses of −60, 0, and +40 pA current injection), and at rest (*bottom*), for an autopatched hippocampal neuron. Access resistance, 55 MΩ; input resistance, 51 MΩ; depth of cell, 1,320 μm. (**e**) Biocytin fill of a representative autopatched cortical pyramidal neuron. Scale bar, 50 μm.
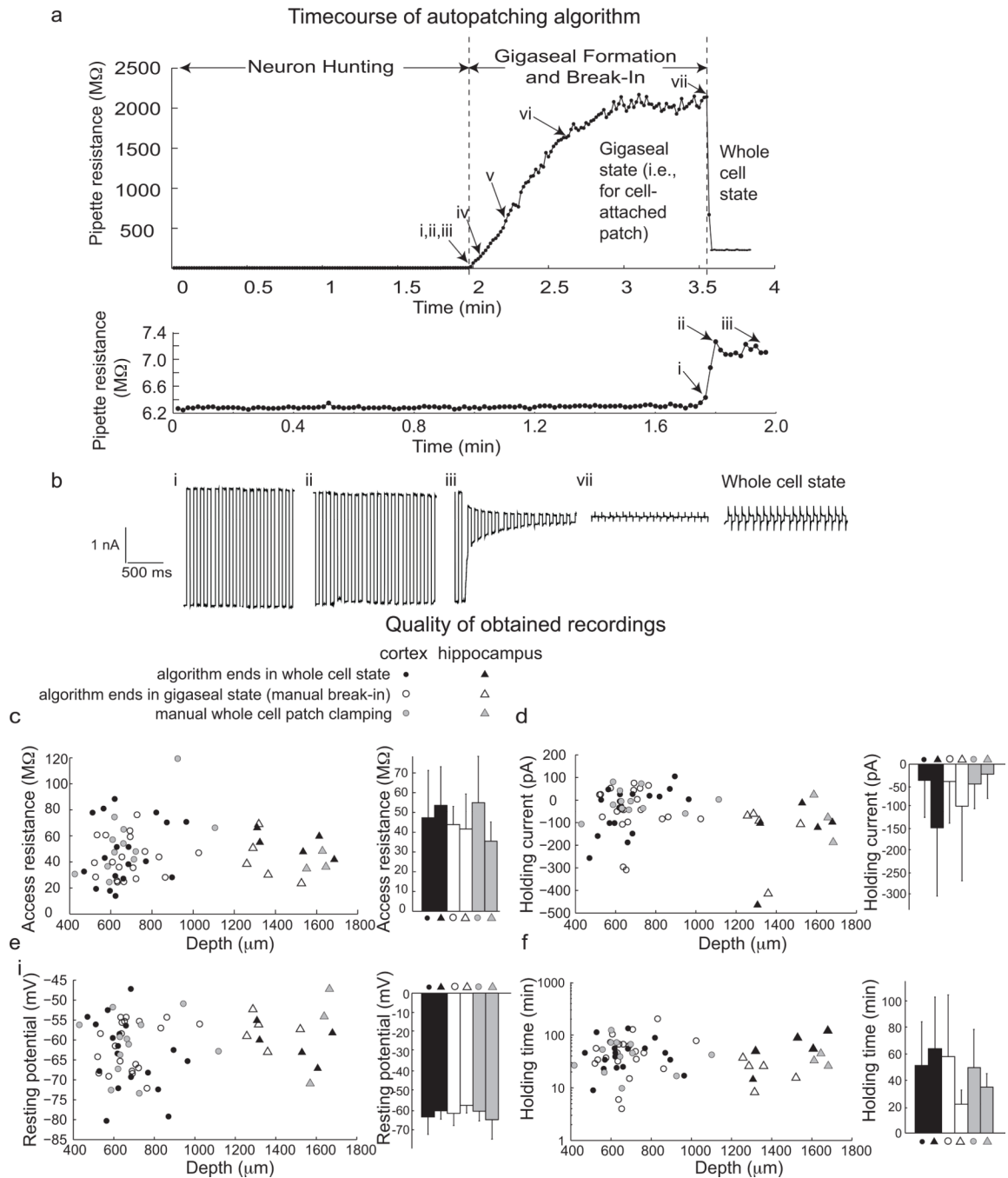
Figure 2. Autopatcher operation and performance

(**a**) Representative timecourse of pipette resistance during autopatcher operation, *top*, with zoomed-in view of the neuron hunting phase, *bottom*. Roman numerals: i, the first of the series of resistance measurements that indicate neuron detection; ii, the last of the series; iii, when positive pressure is released; iv, when suction is applied; v, when holding potential starts to ramp from −30 mV to −65 mV; vi, when it hits −65 mV; vii, break-in. (**b**) Raw traces showing patch pipette currents, while a square voltage wave (10 Hz, 10 mV) is applied, at the events flagged by Roman numerals in **Fig. 2a**. (**c–f**) Quality of recordings obtained with the autopatcher vs. by manual whole cell patch clamping. (**c**) *left,* Plot of

access resistances obtained versus pipette depth and *right*, bar graph summary of access resistances (mean ± s.d.), for the final autopatcher whole cell patch validation test set (closed symbols; $n = 23$), the test set in which the autopatcher concludes in the gigaseal state (open symbols, $n = 24$; data acquired after manual break-in), and the test set acquired via manual whole cell patch clamp (grayed symbols; $n = 15$), for cortical (circles) and hippocampal (triangles) neurons. (**d**) *left*, Resting potential versus pipette depth, and *right*, summary data, plotted as in **c**. (**e**) *left*, Holding current versus pipette depth, and *right*, summary, plotted as in **c**. (**f**) *left*, Holding times versus pipette depth, and *right*, summary, plotted as in **c** (including recordings that were deliberately terminated, as well as recordings terminated spontaneously).